

## Observation of plastic deformation in freestanding single crystal Au nanowires

Dongyun Lee

*Columbia Nanomechanics Research Center, Columbia University, New York, New York 10027  
and Department of Mechanical Engineering, Columbia University, New York, New York 10027*

Manhong Zhao

*Columbia Nanomechanics Research Center, Columbia University, New York, New York 10027  
and Department of Civil Engineering and Engineering Mechanics, Columbia University, New York, New York 10027*

Xiaoding Wei

*Columbia Nanomechanics Research Center, Columbia University, New York, New York 10027  
and Department of Mechanical Engineering, Columbia University, New York, New York 10027*

Xi Chen

*Columbia Nanomechanics Research Center, Columbia University, New York, New York 10027  
and Department of Civil Engineering and Engineering Mechanics, Columbia University, New York, New York 10027*

Seong C. Jun and James Hone

*Department of Mechanical Engineering, Columbia University, New York, New York 10027*

Erik G. Herbert and Warren C. Oliver

*MTS Systems Corporation, Oak Ridge, Tennessee 37830*

Jeffrey W. Kysar<sup>a)</sup>

*Columbia Nanomechanics Research Center, Columbia University, New York, New York 10027  
and Department of Mechanical Engineering, Columbia University, New York, New York 10027*

(Received 19 May 2006; accepted 2 August 2006; published online 14 September 2006)

Freestanding single crystal nanowires of gold were fabricated from a single grain of pure gold leaf by standard lithographic techniques, with center section of 7  $\mu\text{m}$  in length, 250 nm in width, and 100 nm in thickness. The ends remained anchored to a silicon substrate. The specimens were deflected via nanoindenter until plastic deformation was achieved. Nonlocalized and localized plastic deformations were observed. The resulting force-displacement curves were simulated using continuum single crystal plasticity. A set of material parameters which closely reproduce the experimental results suggests that the initial critical resolved shear stress was as high as 135 MPa. © 2006 American Institute of Physics. [DOI: [10.1063/1.2354033](https://doi.org/10.1063/1.2354033)]

Experiments show that the stress at which irreversible, or plastic, deformation initiates in bulk metals is typically independent of the size of the specimen. This is due to the fact that the characteristic length scales of the various physical mechanisms which govern plastic deformation—be they dislocations, twinning, grain boundary sliding, among others—are much smaller than the bulk length scale so that they can be thought of as being continuously distributed in bulk materials and not dependent upon the details of the geometry or loading. However, when the specimen size is sufficiently small, the length scales associated with the deformation mechanisms may become important and lead to a change in the so-called yield stress at which the deformation mechanisms are activated. Length scales and phenomena which can affect yield stress include grain size, specimen size, presence of large strain gradients, and presence of passivation layer, as reviewed by others.<sup>1,2</sup> There are many experimental methods to measure the mechanical properties of metals at small length scales. The two most pertinent to this study are the microcolumn compression test<sup>3</sup> which can test submicron specimens and the deflective tensile test in which

a suspended bridgelike specimen is deflected with a nanoindenter.<sup>4</sup>

In this letter, the mechanical behavior of nanoscale single crystals of gold is reported. The experiments were performed by measuring the force-displacement response associated with deflecting a thin film of gold suspended above a silicon substrate in a double-cantilever configuration with a nanoindenter. Commercially available gold leaf (Monarch™ 24 carat, Sepp Leaf Products, Inc.) with an as-received thickness of about 150 nm as measured by atomic force microscopy was employed in the study. The leaf was glued onto a (001) Si wafer with epoxy in tetrahydrofuran ( $\text{C}_4\text{H}_8\text{O}$ ) solution by spin coating, followed by flattening with a smooth glass surface to obtain a final thickness of about 100 nm. The grain size and crystallographic orientation of the gold leaf were measured by electron backscatter diffraction (EBSD) with a JEOL 5600 scanning electron microscopy (SEM) using CHANNEL 5 software (HKL Technology Inc.). The leaf was comprised of relatively large grains with in-plane dimensions of several tens of micrometers. The out-of-plane crystallographic texture was strongly  $\langle 100 \rangle$ .

Since the in-plane grain size was significantly larger than the desired specimen size, an array of dog-bone-shaped

<sup>a)</sup>Electronic mail: [jk2079@columbia.edu](mailto:jk2079@columbia.edu)

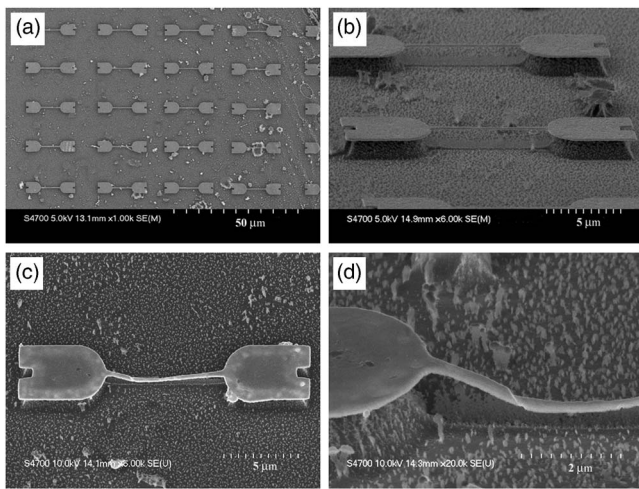


FIG. 1. Nanoscale gold single crystal specimens: (a) array, (b) closeup of specimens, (c) deformed specimen 2, and (d) closeup of specimen 2.

specimens was fabricated within an individual grain, so that the specimens consisted of single crystals of the same orientation. The fabrication regimen was as follows. Positive polymethylmethacrylate electron beam resist was deposited on the film to allow electron beam masking. After developing the resist to expose the portion of the film to become the specimens, a 40 nm thick Ni film was deposited by thermal vapor deposition (Auto 306, BOC Edwards Inc.). The remaining resist under the Ni film was lifted off to leave the Ni deposited directly onto the gold to act as a mask for subsequent processing. The excess leaf was removed by inductively coupled plasma (ICP) etching (anisotropic Ar sputtering mode, Oxford PlasmaLab 80 Plus ICP 65) and the gold thin films were suspended by isotropic  $\text{CF}_4/\text{O}_2$  reactive ion etching (RIE) (gas pressure of 250 mTorr, 200 W, RF power, Technics Series 800 RIE) of the underlying silicon substrate followed by the removal of the Ni film by wet etching. The resulting array of specimens is shown in Figs. 1(a) and 1(b). The gauge length of the specimens was  $7 \mu\text{m}$  and the cross-sectional width was 250 nm. The average thickness was  $105.5 \pm 9.9 \text{ nm}$  as measured in more than ten regions of the specimens via SEM micrographs.

Deformation was induced by deflecting the suspended bridgelike specimens toward the substrate at a rate of 30 nm/s using a nanoindenter (Nanovision<sup>TM</sup>, MTS Systems Corporation, Oak Ridge, TN). A Berkovich indenter with a tip radius of approximately 300 nm was employed. Three specimens were tested. Figure 1(c) shows specimen 2 after the loading. While it is believed that the indenter tip lay along the centerline of the specimen longitudinally, the point of contact was approximately  $0.5 \mu\text{m}$  from the midpoint between the two anchors. It is apparent that plastic deformation occurred heterogeneously, but in a predominantly nonlocalized manner, along the gauge length of the specimen. Figure 1(d) shows a slip localization on a single slip system of specimen 2, which will be discussed later. The force-displacement curves for the three freestanding single crystal gold specimens are shown in Fig. 2(a). In the elastic range, the magnitude of the force was expected to scale with the cube of displacement once the displacement of the bridge became comparable to its thickness.<sup>5</sup> It can be seen that the initial response of all the tested specimens was similar until a load of about  $1 \mu\text{N}$  had been achieved after which the

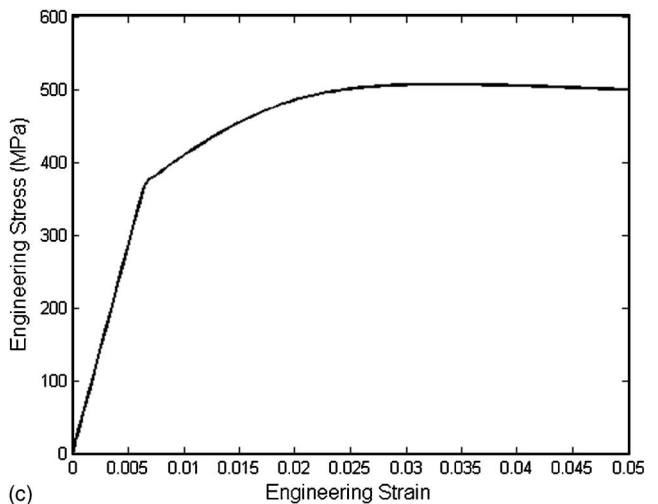
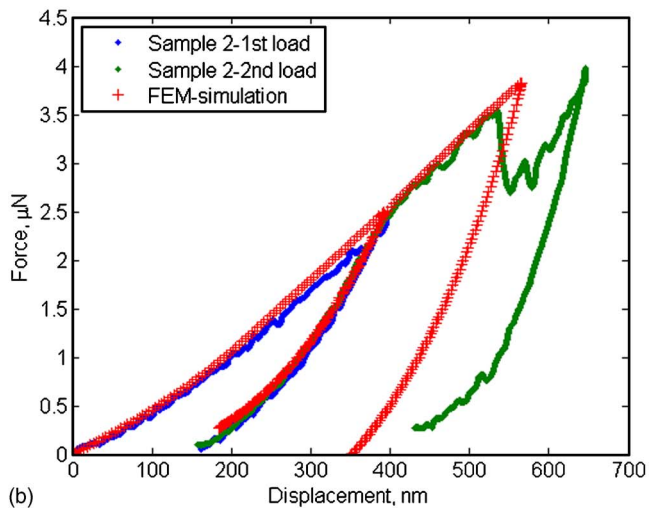
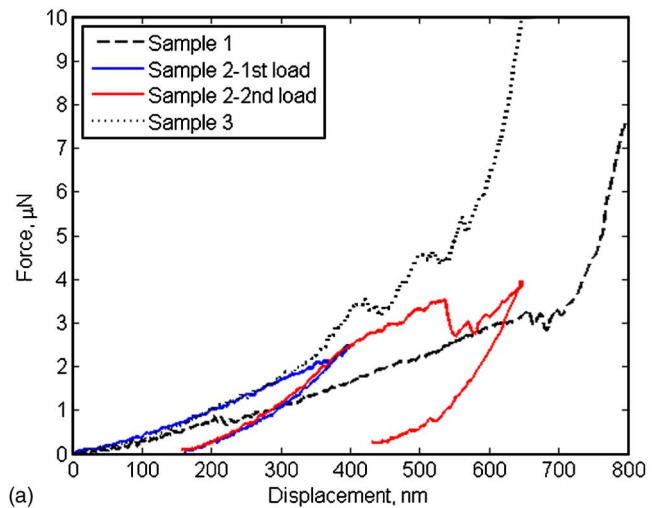


FIG. 2. (Color online) Results of experiments and simulations: (a) experimental force vs displacement data, (b) comparison of finite element results to experimental data, and (c) predicted uniaxial stress-strain response based.

sample 1 suffered a slight load drop. It is assumed that the load drop corresponded to the onset of plastic deformation in that specimen, especially since the force increased at a slower rate than the other two specimens upon further loading. The force-displacement curves for the other two specimens closely followed each other until a load of about  $1.7 \mu\text{N}$  when the slope of the curve for specimen 2 began to decrease which presumably signaled the initiation of plastic

deformation in specimen 2. Specimen 3 experienced a sudden load drop at about  $3.5 \mu\text{N}$ . In addition to a monotonic loading, sample 2 was unloaded after achieving a load of  $2.5 \mu\text{N}$ . It is assumed that the deformation at these relatively small loads occurred in a nonlocalized manner as has been seen in submicron diameter compression specimens.<sup>3</sup> Upon reloading, the specimen experienced a sudden load drop at about  $3.5 \mu\text{N}$  which was likely precipitated by the formation of the slip localization in Fig. 1(d).

Since the plastic slip occurred in a nonlocalized manner in the early stages of the deformation a continuum analysis of the deformation was warranted, with the goal to determine the overall stress and strain response of the material in order to ascertain the approximate mechanical properties of the specimens. Numerical simulations were performed using the commercial finite element code ABAQUS (Ref. 6) with a user-material subroutine incorporating single crystal plasticity.<sup>7</sup> The dimensions of the single crystal in the analysis were 7000 nm in length, 250 nm in width, and 100 nm in thickness. The finite element mesh was comprised of 28 320 eight-node linear hybrid elements with reduced integration and hourglass control.<sup>6</sup> An indenter, modeled as a rigid contact surface, was positioned on the specimen at a point 3000 nm from one end of the gauge section; it had a conical shape with half apex angle  $\alpha=70.3^\circ$  to have the same cross-sectional area to depth ratio as the Berkovich indenter. Additionally, the indenter tip was rounded with a radius of a nominal 60 nm; however, the results were insensitive to the precise radius chosen. The Coulomb friction law was used between contacting surfaces, and the friction coefficient was taken to be 0.15. The elastic moduli of the gold were  $C_{11}=186 \text{ GPa}$ ,  $C_{12}=157 \text{ GPa}$ , and  $C_{44}=42.0 \text{ GPa}$  and the plastic slip systems were  $\{111\}\langle 110 \rangle$ .<sup>8</sup> The crystallographic orientation of the surface normal (parallel to the direction of motion of the indenter) was taken to be  $[001]$  based upon the EBSD analysis. The crystallographic orientation along the gauge length of the specimen was taken to be  $\langle \bar{1} 5.67 0 \rangle$  which is rotated about  $10^\circ$  from  $[010]$ , consistent with the EBSD results and also with the orientation of the slip localization  $\{111\}$  slip plane in Fig. 1(c). The constitutive relation was considered to be rate-independent in the limit of rate dependent viscoplasticity.<sup>9</sup> Specifically, the rate of slip,  $\dot{\gamma}^{(\alpha)}$ , of slip system  $\alpha$  was determined as

$$\dot{\gamma}^{(\alpha)} = \dot{\alpha}^{(\alpha)} \operatorname{sgn}(\tau^{(\alpha)}) \left| \frac{\tau^{(\alpha)}}{g^{(\alpha)}} \right|^n, \quad (1)$$

where  $\tau^{(\alpha)}$  was the resolved shear stress,  $\dot{\alpha}^{(\alpha)}$  the reference strain rate,  $g^{(\alpha)}$  the current strength of slip system  $\alpha$ , and  $n$  the rate sensitivity exponent. The rate of increase of strength of the slip systems was  $\dot{g}^{(\alpha)} = \sum_{\beta} h_{\alpha\beta} \dot{\gamma}^{(\beta)}$ , where the  $h_{\alpha\beta}$  contained the so-called hardening moduli. A simple phenomenological functional form for the hardening moduli given by<sup>10</sup>

$$h_{\alpha\alpha} = h(\gamma) = h_0 \sec h^2 \left| \frac{h_0 \gamma}{\tau_s - \tau_0} \right| \quad (\text{no sum on } \alpha) \quad (2)$$

was used, where  $h_0$  is the initial hardening modulus,  $\tau_0$  the yield stress which equals the initial value of current strength

$g^{(\alpha)}$ ,  $\tau_s$  the stage I stress (or the breakthrough stress where large plastic flow initiates), and  $\gamma = \sum_{\alpha} \int_0^t |\dot{\gamma}^{(\alpha)}| dt$ , where  $t$  is the elapsed time of the simulation. The values  $\dot{\alpha}^{(\alpha)} = 10^{-3}$  and  $n=50$  were used in the simulation. A set of parameters given by  $h_0=2 \text{ GPa}$ ,  $\tau_0=134.2 \text{ MPa}$ , and  $\tau_s=189.0 \text{ MPa}$  closely approximated the mechanical response of specimen 2, as seen in Fig. 2(b) so that the initial critical resolved shear stress on the plastic slip systems was approximately 135 MPa. The uniaxial response of the specimen in  $\langle \bar{1} 5.67 0 \rangle$  was then approximated using these parameters in a plane stress simulation in which the length of the specimen was ten times longer than its width. The results of that simulation are in Fig. 2(c), where it is evident that the tensile yield stress would be approximately 375 MPa and that maximum value of tensile stress would reach about 500 MPa after several percent strain.

In conclusion, previous uniaxial compression experiments<sup>11,12</sup> on 400 nm diameter gold single crystals in the  $\langle 010 \rangle$  direction (oriented  $10^\circ$  from the specimens in the present experiments) experienced similar values of maximum uniaxial stress, around 500 MPa. The data in the present set of experiments are also interesting because it represents a well-defined deformation due to both bending and tension, so that it is complementary to the uniaxial compression tests which do not have significant bending. Finally, it is noted that the force-displacement data of the other two specimens tested in this experiment have different values of stress at which plastic deformation began, which suggests that the plastic behavior at these small length scales can be highly sensitive to slight variations in specimen geometry or loading conditions.

Support from AFOSR FA5550-06-1-0214 and NSF CMS-0134226 and NSF CMS-0407743 is gratefully acknowledged. In addition, this work has used the shared experimental facilities that are supported primarily by the MR-SEC Program of the National Science Foundation under Award No. DMR-0213574 and by the New York State Office of Science, Technology and Academic Research (NYSTAR).

<sup>1</sup>E. Arzt, *Acta Mater.* **46**, 5611 (1998).

<sup>2</sup>O. Kraft, L. B. Freund, R. Phillips, and E. Arzt, *MRS Bull.* **27**, 30 (2002).

<sup>3</sup>M. D. Uchic, D. M. Dimiduk, J. N. Florando, and W. D. Nix, *Science* **305**, 986 (2004).

<sup>4</sup>H. D. Espinosa, B. C. Prorok, and M. Fischer, *J. Mech. Phys. Solids* **51**, 47 (2003).

<sup>5</sup>S. D. Senturia, *Microsystem Design* (Kluwer Academic, Boston, 2001), pp. 239–265.

<sup>6</sup>ABAQUS, ABAQUS 6.4 User's Manual (ABAQUS, Pawtucket, RI, 2004).

<sup>7</sup>Y. Huang, *Internal Report* (Harvard University, Cambridge, MA, 1991), Vol. MECH-178, pp. 1–46.

<sup>8</sup>J. P. Hirth and J. Lothe, *Theory of Dislocations*, 2nd ed. (Krieger, Malabar, FL, 1992), p. 837.

<sup>9</sup>J. W. Hutchinson, *Proc. R. Soc. London, Ser. A* **348**, 101 (1976).

<sup>10</sup>D. Peirce, R. J. Asaro, and A. Needleman, *Acta Metall.* **30**, 1087 (1982).

<sup>11</sup>J. R. Greer, W. C. Oliver, and W. D. Nix, *Acta Mater.* **54**, 1705 (2006).

<sup>12</sup>J. R. Greer, W. C. Oliver, and W. D. Nix, *Acta Mater.* **53**, 1821 (2005).